Two-Dimensional Shock-on-Shock Interaction Problem

PAUL KUTLER,* LEONIDAS SAKELL,† AND GENE AIELLO‡
Ames Research Center, NASA, Moffett Field, Calif.

The unsteady, inviscid flowfield that results when a supersonic vehicle strikes a planar oblique shock wave, though difficult to simulate experimentally, is quite easy to model and compute numerically. The complicated flowfield, which contains multiple shock wave interactions, is determined using a second-order, shock-capturing, finite-difference approach which solves the time-dependent Euler equations under a self-similar transformation. A series of numerical results for a simple two-dimensional wedge is presented which describes the entire disturbed region, including the wave structure, and shows good agreement with the available two- and three-dimensional experimental data.

Introduction

A PROBLEM that has received renewed interest in the past year is the determination of the unsteady, inviscid flowfield that results when a supersonic vehicle (at Mach number M_v) intercepts a planar oblique shock wave traveling in the opposite direction (at Mach number M_i) as shown in Fig. 1. Such an encounter has received considerable attention in the past because of the vulnerability of the vehicle and the belief that the blast-induced transient pulse produced at its surface could conceivably destroy the primary structure. Of late, however, a somewhat different problem has emerged: Can a relatively weak incident shock wave ($p_i/p_\infty < 2$) induce destructive high frequency responses in the secondary structure and appended equipment capable of destroying the vehicle?

The wave structure for a typical three-dimensional shock-on-shock (S-O-S) encounter is shown in Fig. 2. It consists of a multitude of shock waves and slip surfaces which interact to create a rather complicated flowfield. The two-dimensional problem, of which the numerical solution is presented in this paper, is depicted in Fig. 3a. The resulting postinteraction flowfield is shown in Fig. 3b.

The intersection of the incident shock with the original wedge shock yields a refracted wedge shock, a transmitted incident shock, and a slip surface. The transmitted shock that strikes the body is reflected and then struck by the slip surface. The refracted wedge shock and reflected incident shock intersect and result in a single shock and slip surface. This shock curves to meet the new wedge shock at the sonic circle, in front of which exists newly established wedge flow. Known regions of uniform flow are labeled (1) through (4) in Fig. 3b; (1) is the freestream, (2) is the preinteraction wedge flow, (3) is the uniform flow behind the incident shock, and (4) is the postinteraction wedge flow. For purposes of this paper, upstream refers to Regions (1) and (2) and downstream to Regions (3) and (4).

The region of the flowfield of most interest from the numerical solution is at the body in the vicinity of the transmitted incident shock. This shock can reflect regularly or possess a Mach stem, depending on the incident shock inclination. Interest centers around the incident shock angle that yields transition between regular and Mach reflection of the transmitted shock at the body,

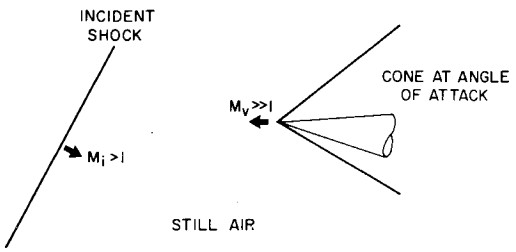

Fig. 1 Three-dimensional shock-on-shock problem.

for it is this encounter angle that results in the largest surface pressure behind the impinging shock. In addition to the peak surface pressure, the numerical solution permits prediction of the time history of pressure on the vehicle during the initial moments of engulfment, thus allowing the aerodynamic forces and moments to be calculated. The two-dimensional problem discussed in this paper is serving as a stepping stone to the more complicated three-dimensional one, but hopefully, during the interim, can provide some enlightening answers.

One of the first theoretical analyses of the S-O-S problem was performed by Smyrl.[1] With the aid of water table experiments, he postulated three types of interaction flowfield patterns: non-intersecting tangents, intersecting tangents, and a single intersecting tangent. Using a small perturbation analysis he obtained closed-form solutions for the pressure distribution in the region bounded by the sonic circle and the impinging shock wave. He considered the impingement of planar shocks of arbitrary strength on thin airfoils, wedges at small angles of attack, and wedges at yaw to the plane of the impingement shock.

Blankenship[2] performed a similar small perturbation analysis. He considered the head-on interaction of an arbitrary strength impingement shock and a slender supersonic cone. In addition to

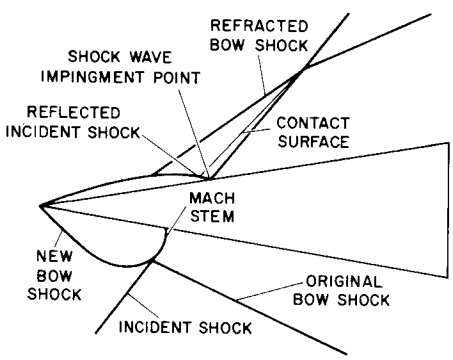

Fig. 2 Typical shock wave and contact surface structure for shock-on-shock problem.

Presented as Paper 74-524 at the AIAA 7th Fluid and Plasma Dynamics Conference, Palo Alto, Calif., June 17–19, 1974; submitted June 18, 1974; revision received September 23, 1974.

Index categories: Aircraft Aerodynamics (Including Component Aerodynamics); Shock Waves and Detonations; Supersonic and Hypersonic Flow.

* Research Scientist, Ames Research Center; Associate Fellow AIAA.

† Senior Engineer, Martin Marietta Aerospace, Orlando Division; Member AIAA.

‡ Staff Engineer, Martin Marietta Aerospace, Orlando Division.

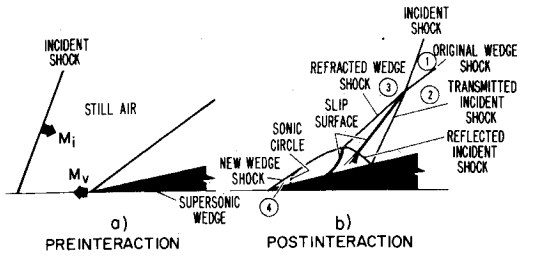

Fig. 3 Pre- and postinteraction wave patterns for two-dimensional shock-on-shock problem.

pressure distributions in the elliptic region, he obtained an expression for the duration of the transient pressure pulse produced by the S-O-S interaction.

Several methods of approximating the S-O-S interaction flowfields were considered by Hudgins and Friedman.[3] They studied weak incident shocks interacting with supersonic cones.

Gardiner[4] has developed a computer code to give an approximate analysis of the three-dimensional S-O-S problem for regular and Mach stem reflections. The conical shock layer of the vehicle is replaced by a two-dimensional (constant property) shock layer having a shock angle that is the same as the conical shock angle of the original vehicle. In the Mach stem analysis he predicts an upper and lower bound (MDAC theories 1 and 2). The upper bound is obtained by assuming the refracted transmitted shock to be normal to the vehicle surface across the entire shock layer; the lower bound is obtained by assuming that only an infinitesimal Mach stem exists at the impingement point of the transmitted wave.

The regular reflection analysis (MDAC theory 3) first calculates the interaction of the incident shock and bow shock, assuming that the shock layer is uniform. The pressure in this layer is assumed to be that which exists just behind the conical bow shock, thus providing the necessary upstream conditions to determine the flow behind the reflected transmitted shock at the surface. The actual nonuniformity of the shock layer in this calculation is accounted for by using a surface compression factor based on a parametric study of cone half-angle and freestream Mach number effects.

A similar analysis has been developed by Martin Marietta Aerospace.[5] For the Mach reflection regime, upper and lower bounds (MMA theories 1 and 2) of the peak surface pressure are computed by assuming that the transmitted shock is straight and normal to the vehicle surface in the entire shock layer or that the transmitted shock bends at the incident shock-bow shock intersection point and is transmitted without loss of strength to the surface, where an infinitesimal Mach stem is assumed to exist. The upper bound theory first calculates the incident shock normal velocity component with respect to the vehicle at rest. The Mach stem velocity with respect to the air is then set equal to the component of the velocity along the vehicle surface. The lower bound theory assumes that the velocity is that of the refracted incident shock with respect to the vehicle surface. Different assumptions are used in analyzing the regular reflection regime (MMA theory 3). The shock layer is considered as a constant pressure region. The value of pressure is set equal to that behind the bow shock for the interaction calculation, while it is set equal to the surface pressure of the vehicle for the reflection angle calculation. In addition to the above, a computer code[6] (SLAN) exists that incorporates empirical data and curve-fits to analyze the interaction region and predict peak pressures.

There have been many experimental investigations of the S-O-S problem.[7-14] They have produced both flowfield photographs and pressure-time histories of the interaction region, which has served as the only means of comparing the accuracy of the various theoretical approaches.

Two broad weaknesses exist in the available theoretical results: 1) each theoretical approach involves some sort of simplifying assumption about the interaction flowfield (e.g., weak blast waves, thin or slender vehicles, replacement of a nonuniform shock layer by a uniform one, etc.) and 2) none of the approaches completely describes the entire flowfield. Further, the uncertainties in peak pressure, pulse duration, etc., are unacceptable in terms of the concomitant structural response. As for the experimental approaches, it is extremely difficult not only to set up a given encounter (e.g., to ensure required blast conditions) but also to record the pressure-time history at the vehicle surface. In light of these weaknesses, a more accurate approach is needed to perform a complete parametric study of the S-O-S problem for a three-dimensional or axisymmetric vehicle. This paper hopefully fills that need.

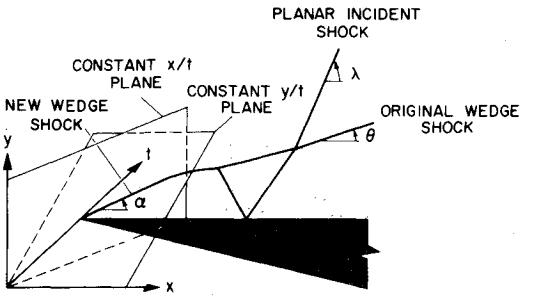

Fig. 4 Self-similar planes.

Because of the multiplicity of discontinuities and their interactions that occur in the S-O-S problem, our approach is to use the "shock-capturing technique"[15-17] (SCT) which allows for the existence and natural formation of such discontinuities and does not require any special treatment of them. Admittedly, solution by a "sharp shock" approach is conceivable, but to allow for all possible shock patterns would be a formidable task.

The basis for solution of this unsteady problem relies on the fact that the flowfield is self-similar with respect to time, i.e., as time increases, the wave structure and flowfield expand linearly (assuming that at $t = 0$ the incident shock is at the wedge tip). Thus in constant x/t and y/t planes (with x along and y normal to the surface of the wedge as shown in Fig. 4) the flowfield is invariant with time. This self-similarity is generated as a result of there being no characteristic length associated with the body and the fact that the incident shock wave is planar. Thus, by applying the appropriate self-similar transformation to the unsteady gasdynamic equations, the unsteady problem can be made steady and solved as an initial value problem using conventional finite difference procedures.

Governing Equations

The basic orthogonal coordinate system that is used for the two-dimensional problem is Cartesian, the origin of which is located at the wedge vertex with the x-axis along and the y-axis normal to the surface of the wedge (see Fig. 5). It has been shown[18,19] that when using the shock-capturing approach, if the coordinate directions can be chosen to be coincident with the captured shocks, the associated post- and precursor oscillations

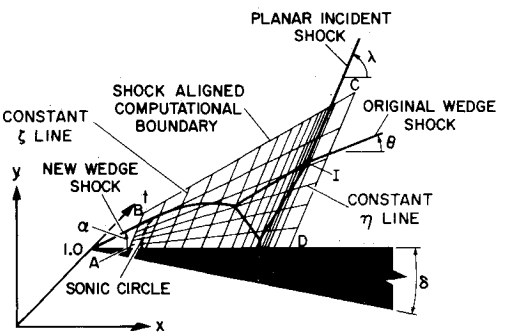

Fig. 5 Computational mesh.

will be minimized. In this problem it is possible, using a nonorthogonal coordinate transformation, to align the incident shock, the original wedge shock, and the new wedge shock with coordinate directions. Furthermore, since our main interest in the solution of this problem is to resolve the flowfield in the vicinity of the transmitted shock impingement point, another transformation can be applied to cluster points in that region.[20] As mentioned in the introduction, we must also include in the final transformation the fact that the flowfield is self-similar with respect to time. Thus, the resulting transformation from (t, x, y) to (τ, ζ, η) space, which satisfies the above criteria, is as follows:

$$\tau = t$$

$$\zeta = \begin{cases} C + \dfrac{1}{\beta}\sinh^{-1}\left[\left(\dfrac{\xi}{\xi_c} - 1\right)\sinh \beta C\right] & \beta > 0 \\ \xi & \beta = 0 \end{cases} \tag{1}$$

$$\eta = y/x \tan\theta$$

where

$$\xi = [x - f(t, y)/t]$$

$$C = \frac{1}{2\beta}\ln\left[\frac{1 + (e^{\beta} - 1)\xi_c/\xi_{\max}}{1 - (1 - e^{-\beta})\xi_c/\xi_{\max}}\right]$$

$$f(t, y) = y/\tan\lambda + \dot{x}_b t$$

and where λ = incident shock angle (see Fig. 4), θ = original wedge shock angle (see Fig. 4), $\dot{x}_b$ = velocity of left-hand boundary of computational plane, $\xi_c = \xi$ value about which points are to be clustered, $\xi_{\max}$ = maximum value of ξ, and β = clustering parameter; concentration of points increases with β. Applying this transformation to the two-dimensional time-dependent Euler equations yields the following partial differential equation:

$$U_\tau + E_\zeta + F_\eta + H = 0 \tag{2}$$

where

$$U = \tau^2(\dot{x}_b + \xi)U^* \tan\lambda$$

$$E = \tau(\dot{x}_b + \xi)\{[E^* - (\dot{x}_b + \xi)U^*]\tan\lambda - F^*\}\zeta_\xi$$

$$F = \tau(\tan\lambda - \eta\tan\theta)(F^*/\tan\theta - \eta E^*)$$

$$H = 2\tau(F^* - \eta E^*\tan\theta) - \tau(\dot{x}_b + \xi)\{[E^* - (\dot{x}_b + \xi)U^*]\tan\lambda - F^*\}\zeta_{\xi_c}$$

and

$$\zeta_\xi = \frac{\xi_{\max}\sinh\beta C}{\xi_c\beta\{1 + [(\xi/\xi_c - 1)\sinh\beta C]^2\}^{1/2}}$$

$$\zeta_{\xi_c} = \frac{-(\xi/\xi_c - 1)\sinh^2\beta C}{\xi_c\{1 + [(\xi/\xi_c - 1)\sinh\beta C]^2\}}$$

$$U^* = \begin{bmatrix} \rho \\ \rho u \\ \rho v \\ e \end{bmatrix}, \quad E^* = \begin{bmatrix} \rho u \\ p + \rho u^2 \\ \rho uv \\ (e + p)u \end{bmatrix}, \quad F^* = \begin{bmatrix} \rho v \\ \rho uv \\ p + \rho v^2 \\ (e + p)v \end{bmatrix}$$

In Eq. (2) p represents the pressure; ρ, the density; u and v, the velocity components in the x and y directions; and e, the total energy per unit volume. The energy e is related to p, ρ, u, and v for an ideal gas by the following equation:

$$e = p/(\gamma - 1) + \rho(u^2 + v^2/2) \tag{3}$$

Equation (2) is hyperbolic with respect to τ and can be solved iteratively, e.g., in a $\tau = 1$ plane, using a finite difference scheme. Convergence of iterations is recognized when the U_τ terms of Eq. (2) vanish.

The transformation given by Eq. (1) results in the computational plane shown in Fig. 5. The left-hand boundary (A-B) is chosen to be downstream of the sonic circle or in the uniform regions of newly established wedge flow and postinteraction conditions [Regions (3) and (4) of Fig. 3], while the right-hand boundary (C-D) is chosen to be upstream of the intersection point of the incident shock and original wedge shock [Regions (1) and (2) of Fig. 3]. The top boundary of the computational plane (B-C) is chosen to be at an angle greater than the largest angle of the original (θ) or new wedge shock (α), while the lower boundary (A-D) is coincident with the surface of the wedge.

Boundary and Initial Conditions

The correct boundary conditions must be applied at the extremities of the computational plane. At the surface of the wedge (A-D of Fig. 5), the tangency condition ($v = 0$) must be satisfied. Since an iterative procedure is employed to obtain the solution (as opposed to a marching technique in the τ direction), accurate representation of the tangency condition can be obtained by using a simple Euler predictor/modified Euler corrector with one-sided differences in the η-direction,[17,19] for which the tangency condition is imposed after the corrector step.

In order for the problem to be posed properly, the permeable extremities (A-B), (B-C), and (C-D) of Fig. 5 must be hyperbolic boundaries,[19] i.e., the flow through these boundaries with respect to the transformed coordinates must be supersonic. For all of the cases presented in this paper (i.e., those in which the intersection point (I of Fig. 5) of the incident shock and original wedge shock move in the positive x-direction), the boundaries have supersonic inflow. It is also necessary when choosing these boundaries to ensure that they completely encompass the disturbed flow region of interest. For example, the boundary (C-D) of Fig. 5 would still be a supersonic inflow boundary if it were located to the left of point I. Thus, in the actual calculation, (C-D) is chosen to be approximately 10 mesh intervals to the right of point I. Similarly, (B-C) is chosen to be 10 mesh intervals above either the old or new wedge shock, depending on which shock angle is greater. The boundary (A-B) is chosen to be 5 mesh intervals to the left of the sonic circle, where the x intercept of the intersection of the sonic circle and the body is given by the following equation:

$$x_{sc_b} = (q_4 - a_4)t \tag{4}$$

where q_4 and a_4 are the velocity and speed of sound in Region 4. The number of intervals chosen allows adequate space for all shocks to be captured.

Since the permeable boundaries are hyperbolic and in regions of known flow, it is sufficient to specify the flow properties along these boundaries and not allow them to change during the entire integration procedure. Initially, the vehicle Mach number M_v, the wedge angle δ, the incident shock Mach number M_i, its inclination λ, and the freestream pressure and density p_1 and ρ_1, are given. Having these, the flow properties along the boundary (A-B-C-D) can be determined.

The boundary (C-D) crosses regions (1) and (2). Knowing M_v and δ, the two-dimensional supersonic wedge relations yield p_2, ρ_2, $\mathbf{q}_2$, and the shock angle θ. The original wedge shock is located at $\eta = 1$ in the computational plane [see Eq. (1)]. Thus for $\eta < 1$, Region 2 properties are assigned, while for $\eta > 1$, Region 1 properties (freestream) are used. Table 1 lists the velocity components for these two regions.

Region 1 properties (freestream) are used. Table 1 lists the velocity components for these two regions.

Table 1 Velocity components of constant flow regions and incident shock with respect to wedge ($\mathbf{q}_j = u_j\hat{i} + v_j\hat{j}$)

j	u_j	v_j
1	$q_1\cos\delta$	$-q_1\sin\delta$
2	q_2	0
3	$q_{i_2}\sin\lambda + q_1\cos\delta$	$-(q_{i_2}\cos\lambda + q_1\sin\delta)$
4	q_4	0
is	$q_{i_1}\sin\lambda + q_1\cos\delta$	$-(q_{i_1}\cos\lambda + q_1\sin\delta)$

The boundary (B-C) crosses Regions (1) and (3). Knowing M_i, the following quantities can be found:

$$q_{i_1} = M_i a_1$$

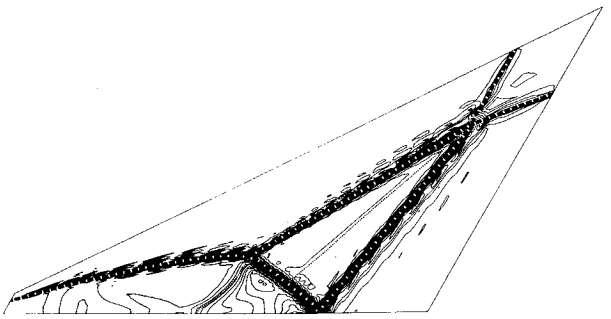

Fig. 6 Density contours for two-dimensional shock-on-shock problem; $M_v = 3.15$, $\delta = 30°$, $M_i = 2$, $\lambda = 60°$, $\beta = 0$.

the velocity of the incident shock with respect to still air;

$$q_{i_2} = q_{i_1}\{1-[(\gamma-1)M_i^2+2]/[(\gamma+1)M_i^2]\}$$

the velocity of the air behind the incident shock with respect to still air; and

$$p_3 = p_1[2\gamma M_i^2-(\gamma-1)]/(\gamma+1)$$
$$\rho_3 = \rho_1(\gamma+1)M_i^2/[(\gamma-1)M_i^2+2]$$

The velocity components for Region (3) are given in Table 1. The location of the incident shock in the computational plane can be found by determining the intersection of it with the original wedge shock. The equation of the incident shock $y_{is} = y_{is}(x,t)$ is

$$y_{is} = (x\sin\lambda - q_{is_n}t)/\cos\lambda \tag{5}$$

where

$$q_{is_n} = q_{is}\cos v \quad \text{(see Table 1 for } q_{is}\text{)}$$
$$v = \pi/2-(\mu+\lambda)$$
$$\mu = \tan^{-1}(u_{is}/v_{is})$$

while the equation of the original wedge shock is

$$y_{ow} = x\tan\theta \tag{6}$$

The solution of Eqs. (5) and (6) in the $\tau = 1$ plane yields x_I and y_I, which, when substituted into Eq. (1), gives the location ζ_I of the incident shock in the computational plane. Thus, along (C-D) for values of $\zeta < \zeta_I$, region 3 properties are assigned while for values of $\zeta > \zeta_I$, freestream conditions are assigned.

The boundary (A-B) crosses Regions (3) and (4). Knowing the flow properties in Region (3) and thus the Mach number M_3 and flow inclination, $\beta = \tan^{-1}(v_3/u_3)$ (see Fig. 6), the supersonic wedge relations yield the flow properties in Region (4) p_4, ρ_4, q_4, and the shock angle α. Having α, Eq. (1) yields the η location of the new wedge shock in the computational plane, above which the flow properties of Region (3) are assigned and below which the flow properties of Region (4) are assigned.

Initially, when $\tau = 1$, the remaining grid points are assigned values of the flow variables equal to those of the freestream. The integration stepsize $\Delta\tau$ is computed from the following equations, which are based on a one-dimensional, amplification matrix, stability analysis[21]:

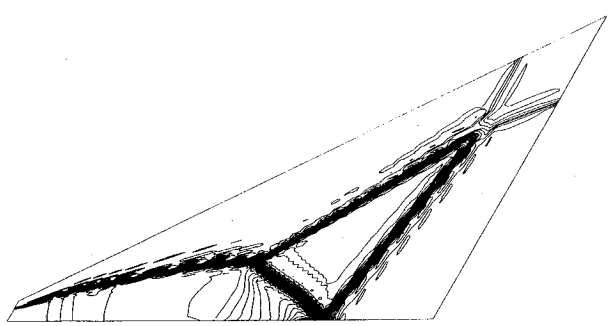

Fig. 7 Pressure contours for two-dimensional shock-on-shock problem; $M_v = 3.15$, $\delta = 30°$, $M_i = 2$, $\lambda = 60$, $\beta = 0$.

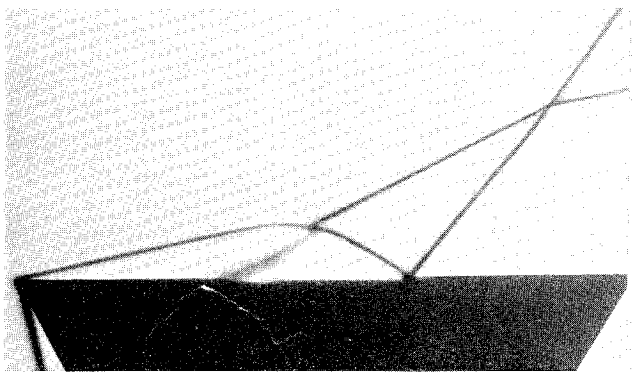

Fig. 8 Schlieren photograph of two-dimensional shock-on-shock problem; $M_v = 3.15$, $\delta = 30°$, $M_i = 2$, $\lambda = 60°$.

$$\Delta\tau_\zeta = \frac{CN\,\Delta\zeta}{\zeta_\xi\left|(-\dot{x}_b-\xi+u-v\cot\lambda)/\tau \pm a\right|_{\max}} \tag{7a}$$

$$\Delta\tau_\eta = \frac{CN\,\Delta\eta}{\left|\dfrac{1-\eta\tan\theta\cot\lambda}{\tau(\dot{x}_b+\xi)}(-\eta u+v\cot\theta)\pm a\right|_{\max}} \tag{7b}$$

$$\Delta\tau = \min(\Delta\tau_\zeta, \Delta\tau_\eta) \tag{7c}$$

where CN is the Courant number and is usually assigned a value of 0.9.

Finite-Difference Scheme

To solve Eq. (2), the second-order, finite-difference scheme of MacCormack[22] is used. It has been demonstrated[15,16,17] that this scheme, when used in the shock-capturing approach, can accurately predict the location and intensity of all flow discontinuities, as well as the continuous portions of the flowfield. Applied to Eq. (2), MacCormack's scheme takes the form:

$$U_{j,k}^{(1)} = U_{j,k}^n - \frac{\Delta\tau}{\Delta\zeta}(E_{j+1,k}^n - E_{j,k}^n) - \frac{\Delta\tau}{\Delta\eta}(F_{j,k+1}^n - F_{j,k}^n) - \Delta\tau H_{j,k}^n \tag{8a}$$

$$U_{j,k}^{n+1} = \frac{1}{2}\left[U_{j,k}^n + U_{j,k}^{(1)} - \frac{\Delta\tau}{\Delta\zeta}(E_{j,k}^{(1)} - E_{j-1,k}^{(1)}) - \frac{\Delta\tau}{\Delta\eta}(F_{j,k}^{(1)} - F_{j,k-1}^{(1)}) - \Delta\tau H_{j,k}^{(1)} + D_{j,k}^n\right] \tag{8b}$$

where

$$U_{j,k}^n = U(n\Delta\tau, j\Delta\zeta, k\Delta\eta)$$
$$E_{j,k}^n = E(U_{j,k}^n, n\Delta\tau, j\Delta\zeta, k\Delta\eta)$$
$$E_{j,k}^{(1)} = E^{(1)}[U_{j,k}^{(1)}, (n+1)\Delta\tau, j\Delta\zeta, k\Delta\eta], \text{ etc.}$$

and $D_{j,k}^n$ is a fourth-order smoothing term, which was sometimes required to damp undesirable oscillations that occurred in the vicinity of the intersection of the incident shock and bow shock and is given by

$$D_{jn,k} = -d_\zeta[U_{j+2,k}^n + U_{j-2,k}^n - 4(U_{j+1,k}^n + U_{j-1,k}^n) + 6U_{j,k}^n] - d_\eta[U_{j,k+2}^n + U_{j,k-2}^n - 4(U_{j,k+1}^n + U_{j,k-1}^n) + 6U_{j,k}^n]$$

where d_ζ and d_η are input constants that control the amount of smoothing.

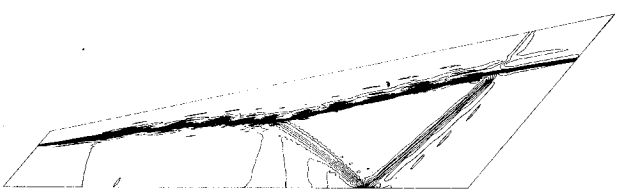

Fig. 9 Pressure contours for two-dimensional shock-on-shock problem; $M_v = 5$, $\delta = 11.2°$, $M_i = 1.24$, $\lambda = 50°$, $\beta = 0$.

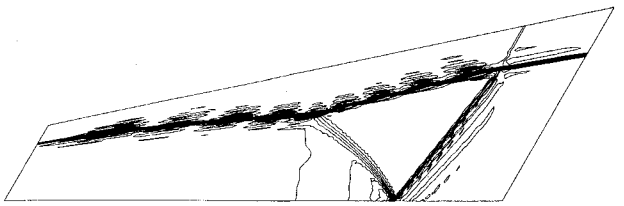

Fig. 10 Pressure contours for two-dimensional shock-on-shock problem; $M_v = 5$, $\delta = 11.2°$, $M_i = 1.24$, $\lambda = 60°$, $\beta = 5$, $\xi_c = 4.24$.

Numerical Results

All computations for the results presented in this section were performed on an IBM 360/67 computer linked with a cathode-ray tube (CRT). The interactive capability of the CRT allowed the flowfield to be displayed after each iteration and also permitted various control parameters such as the Courant number and clustering parameter to be easily changed.

To verify the two-dimensional S-O-S numerical procedure, we chose to model one of the experiments performed by Merritt and Aronson[10] for which Schlieren photographs were available. These photographs show the shock-wave interactions generated by a 30° wedge at Mach 3.15 being struck head-on ($\lambda = 60°$) by a planar incident shock at Mach 2. In the numerical solution, the grid size consisted of 65 points in the ζ-direction and 39 points in the η-direction. For this case, the clustering parameter β was equal to zero. The sonic circle was found to lie close to the nose, and thus resulted in the points being rather close to one another at the left-hand boundary in the physical plane compared to the points at the right-hand boundary. The sonic-circle region thus controlled the maximum allowable stepsize, and this particular calculation required approximately 2000 iterations to converge (about 3 hours of computer time).

The results of this calculation are shown in Figs. 6 and 7 in the form of contour plots of the computational plane. Figure 6 is a density contour plot of the shock interaction region, which clearly shows all the shock waves and slip surfaces. The flow discontinuities that are not aligned with a coordinate direction are spread over approximately 2 mesh intervals, but their precise location can be pinpointed as denoted by the broad white dashed lines (shock waves) and the thin dotted lines (slip surfaces) superimposed on the contour plot. The existence of a slip surface can be demonstrated by comparing the pressure contour shown in Fig. 7 with the density contour of Fig. 6. Since pressure is continuous across the slip surface, the constant pressure lines do not coalesce in the vicinity of the slip surfaces.

The experimental result[10] showing the wave structure for this case is presented in Fig. 8. A comparison of this figure with the density contour of Fig. 6 reveals that, qualitatively, the wave structures are identical but, quantitatively, the positions of some of the waves are in disagreement. The experiment depicts a small Mach stem at the shock impingement point, whereas the numerical solution shows a regular reflection. The disagreement here is probably due to the shock-boundary layer interaction effects. It should also be pointed out that if the original wedge shock in the experiment were extrapolated toward the wedge vertex, it would not intersect it. This indicates that there must have been some nonuniformities in the tunnel flow and this could account for the disagreement in wave locations with the numerical solution.

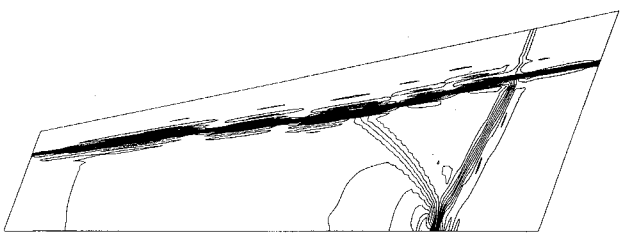

Fig. 11 Pressure contours for two-dimensional shock-on-shock problem; $M_v = 5$, $\delta = 11.2°$, $M_i = 1.24$, $\lambda = 70°$, $\beta = 0$.

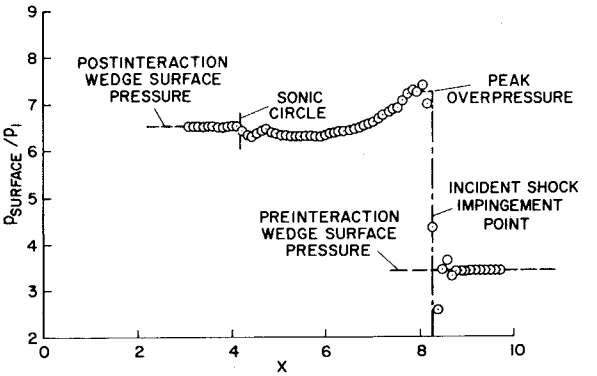

Fig. 12 Surface pressure distribution for two-dimensional shock-on-shock problem; $M_v = 5$, $\delta = 11.2°$, $M_i = 1.24$, $\lambda = 50°$, $\beta = 0$.

A recent test program§ to model the S-O-S problem was conducted at Holloman AFB[14] using a rocket propelled sled. By appropriately timing the detonation of an explosive charge that was suspended above the track, it was possible to achieve a broadside encounter and extract the transient pressure pulse via a telemetry system. The nominal test conditions, which will serve as the basis for the following comparisons between predictive techniques, are as follows:

Table 2 Test conditions

Vehicle:	
Mach No.	5.0
Cone half-angle	11.2°
Altitude	4500.0 ft
Angle of attack	0°
Base diam.	9.0 in.
Incident shock:	
Strength	$p_i/p_\infty = 1.6$ ($M_i \doteq 1.24$)
Orientation	parallel to cone surface ($\lambda = 0°$)

Pressure sensors were located at three axial stations, namely 11, 16, and 21 in. from the apex on the windward ray of the cone.

The two-dimensional shock-capturing code was designed to determine only those flowfields that resulted in the intersection point of the incident shock and original bow shock moving down the body (away from the nose), i.e., those that contained the transition from regular to Mach stem reflection of the transmitted shock. Thus, the broadside case of the Holloman sled tests is not allowed, and only an extrapolation of the SCT numerical results to that condition can be used for comparison purposes.

To that end, a series of numerical solutions were obtained for the Holloman test conditions, but for incident shock angles of $30° \leqq \lambda \leqq 70°$ and not the broadside case of $\lambda = 0°$. All of the numerical solutions used a 65 by 39 grid and required, on the average, 500 iterations to converge (about 45 min of CPU time). Typical pressure contour plots showing one regular and two Mach stem reflections corresponding to λ's of 50°, 60° and 70° are shown in Figs. 9, 10, and 11. The surface pressure distribution for the regular reflection case is shown in Fig. 12. For the $\lambda = 60°$ contour, for which there exists a very small Mach stem, longitudinal point clustering was used, and a plot

§ Participants in the test program, in addition to the Holloman track facility staff, included the Avidyne and Nuclear Sciences Divisions of KAMAN, Ballistic Research Laboratory, and Martin-Marietta Aerospace.

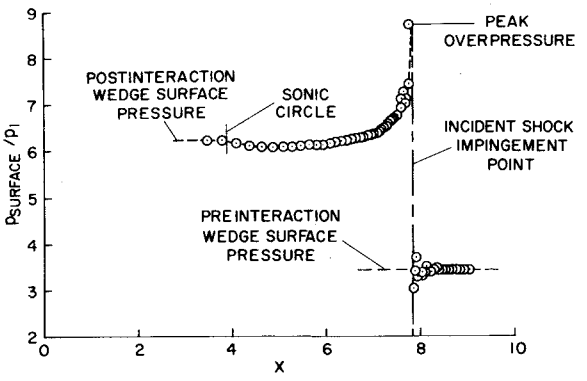

Fig. 13 Surface pressure distribution for two-dimensional shock-on-shock problem; $M_v = 5$, $\delta = 11.2°$, $M_i = 1.24$, $\lambda = 60°$, $\beta = 5$.

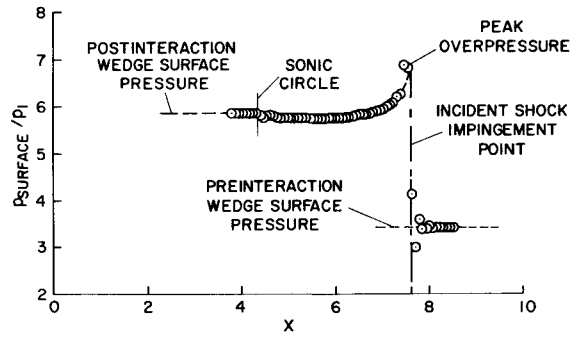

Fig. 14 Surface pressure distribution for two-dimensional shock-on-shock problem; $M_v = 5$, $\delta = 11.2°$, $M_i = 1.24$, $\lambda = 70°$, $\beta = 0$.

of the surface pressure distribution is shown in Fig. 13. Figure 14 shows the surface pressure distribution for the $\lambda = 70°$ case in which a larger Mach stem of the transmitted shock occurred. The pressure downstream of the Mach stem decays exponentially, unlike the regular reflection case in which there is a pressure plateau.

A plot of the peak pressures obtained from the SCT results as a function of the encounter angle $\lambda' = \pi/2 - (\lambda + \delta)$ is shown in Fig. 15, along with the Holloman sled test data and the results of other theories (two dimensions). The tests data indicate a nominal peak of about 96 psi, with a scatter ranging from 83 to 110 psi. The approximate theories shown on this figure include that of Martin-Marietta Aerospace (MMA),[5] a two-dimensional method of characteristic (MOC),[2,3] and that of Gardiner[4] (MDAC). The MMA and MDAC theories 1, 2, and 3 were discussed in the introduction. The MOC approach applies only in the regular reflection regime exclusive of the broadside case and shows excellent agreement with the SCT

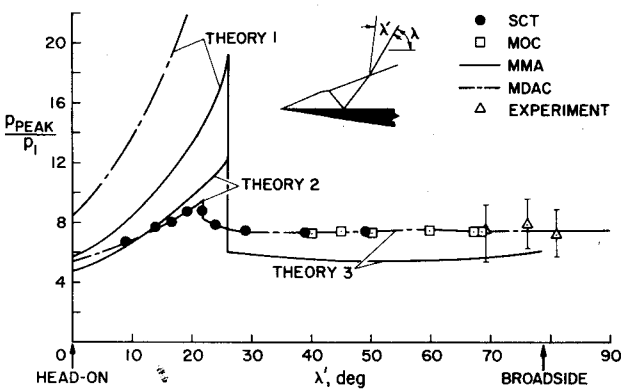

Fig. 15 Variation of predicted values of peak surface pressure with encounter angle for two-dimensional shock-on-shock problem.

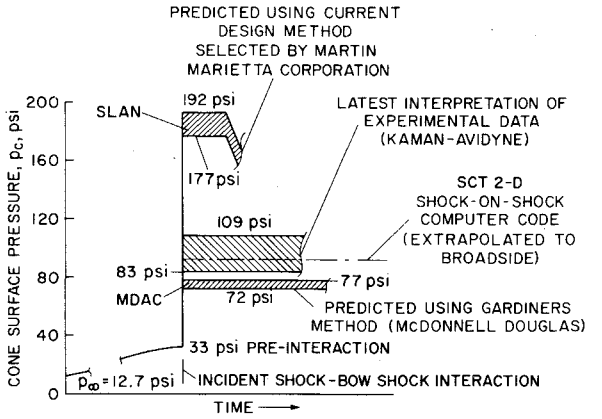

Fig. 16 Comparison of predicted and experimental peak surface pressure on a cone due to shock-on-shock interaction.

results. The MMA model, on the other hand, underpredicts the peak pressure in the near-broadside case, which is probably a result of neglecting the effect of the velocity gradient in the conical flowfield on the wave transmitted to the surface, as suggested by Hayes.[24] Gardiner's lower bound theory agrees quite well with both the SCT and MOC results. Both the SCT and MDAC results show a maximum peak pressure in the vicinity of $\lambda = 20°$ or transition between regular and Mach reflection.

The experimental and theoretical (three-dimensional approximation) peak surface pressures on a cone due to a broadside encounter are shown in Fig. 16. Values predicted by the SLAN code[6] are twice that of the experiment. The SCT (two-dimensional) data extrapolated to broadside agrees quite well with the experiment, falling within the band of experimental data. Gardiner's method slightly underpredicts the peak surface pressure. It should be noted that Gardiner's results shown in this figure were obtained by approximating the three-dimensional conical S-O-S problem using a modified two-dimensional analysis as explained in the introduction, while his results shown in Fig. 15 were based on an unmodified two-dimensional analysis.

Until the three-dimensional model is developed, there will be questions why the two-dimensional analyses agree so well with the cone test data, at least as far as peak pressures are concerned. Taken at face value, one may speculate that the amplification of the transmitted wave due to interaction between it and the conical flowfield, and the concomitant effect on the reflected wave are each approximately equal to the difference in initial surface pressure between the 11.2° cone and the wedge of the same angle so that the resultant peak transient pressure on the two is roughly the same. In any case, the three-dimensional numerical results to be produced during a forthcoming program should clarify these issues.

References

[1] Smyrl, J. L., "The Impact of a Shock-Wave on a Thin Two-Dimensional Aerofoil Moving at Supersonic Speed," *Journal of Fluid Mechanics*, Vol. 15, Feb. 1963, pp. 223–240.

[2] Blankenship, V. D., "Shock-Shock Interaction on a Slender Supersonic Cone," *Journal of Fluid Mechanics*, Vol. 22, July 1964, pp. 599–615.

[3] Hudgins, H. E., Jr. and Friedman, E. M., "Shock-Shock Interaction Studies for Weak Incident Shocks," TR-4590, Dec. 1973, Picatinny Arsenal, Dover, New Jersey.

[4] Gardiner, C. P., Memorandum to J. Xerikos, McDonnell-Douglas Rept. A3-830-BBB1-72-53, Aug. 4, 1972.

[5] Lagow, J. and Murad, P., "A Computerized Model to Predict the Transient Pressure Distribution Due to Shock-Shock Interaction," Martin-Marietta Aerospace, Orlando, Fla., to be published.

[6] Hudgins, H. E., "SLAN, A Computer Program for Estimating Shock Interaction Loading," TR-3676, Apr. 1968, Feltman Research Labs., Picatinny Arsenal, Dover, New Jersey.

[7] Brown, E. A., Jr. and Mullaney, G. J., "Experiments on The

Head-On Shock-Shock Interaction," *AIAA Journal*, Vol. 3, No. 11, Nov. 1965, pp. 2168–2170.

[8] Blankenship, V. D. and Merritt, D. L., "A Note on Experimental and Theoretical Comparisons of Conical Shock-Shock Interactions," *AIAA Journal*, Vol. 4, No. 11, Nov. 1966, pp. 2054–2056.

[9] Damkevala, R. J. and Zumwalt, G. W., "A Technique for Studying Interactions Between a Supersonic Body and Blast Waves Approaching Obliquely," SC-CR-67-2533, May 1967, Sandia Labs., Albuquerque, N. Mex.

[10] Merritt, D. L. and Aronson, P. M., "Wind Tunnel Simulation of Head-On Bow Wave–Blast Wave Interactions," NOLTR 67-123, Aug. 1967, Naval Ordnance Lab., White Oak, Silver Spring, Md.

[11] Baltakis, F. P., Merritt, D. L., and Aronson, P. M., "Two Techniques for Simulating the Interaction of a Supersonic Vehicle with a Blast Wave," NOLTR 67-154, Oct. 1967, Naval Ordnance Lab., White Oak, Silver Spring, Md.

[12] Merritt, D. L. and Aronson, P. M., "Oblique Shock Interaction Experiments," NOLTR 69-108, May 1969, Naval Ordnance Lab., White Oak, Silver Spring, Md.

[13] Baltakis, F. P., "Shock Interaction Surface Pressures for Hemispherical and Conical Bodies," NOLTR 71-27, Feb. 1971, Naval Ordnance Lab., White Oak, Silver Spring, Md.

[14] Ruetenik, J. R., Cole, E. L., Jones, R. E., "Shock-on-Shock Pressure Measurements at Mach 5 from Rocket-Propelled Sled Tests, Phase I: Lateral Intercepts," KAMAN AviDyne Rept. KA TR-98, Aug. 1973, Kaman Aerospace Corp., Bloomfield, Conn.

[15] Kutler, P. and Lomax, H., "Shock-Capturing, Finite-Difference Approach to Supersonic Flows," *Journal of Spacecraft and Rockets*, Vol. 8, No. 12, Dec. 1971, pp. 1175–1182.

[16] Kutler, P., Warming, R. F., and Lomax, H., "Computation of Space Shuttle Flowfields Using Noncentered Finite-Difference Schemes," *AIAA Journal*, Vol. 11, No. 2, Feb. 1973, pp. 196–204.

[17] Kutler, P., "Supersonic Flow in the Corner Formed by Two Interesting Wedges," *AIAA Journal*, Vol. 12, May 1974, pp. 577–578.

[18] MacCormack, R. W. and Warming, R. F., "Survey of Computational Methods for Three-Dimensional Supersonic Inviscid Flows with Shocks," AGARD Lecture Series No. 64 on Advances in Numerical Fluid Dynamics, Feb. 1973.

[19] Kutler, P., "Computation of Three-Dimensional, Inviscid Supersonic Flows," lecture notes from AGARD/VKI Short Course on "Computational Methods in Fluid Dynamics," Feb. 1974, to be published in *Lecture Notes in Physics*.

[20] Thomas, P. D., Vinokur, M., Bastianon, R., and Conti, R. J., "Numerical Solution for the Three-Dimensional Inviscid Supersonic Flow of a Blunt Delta Body," *AIAA Journal*, Vol. 10, No. 7, July 1972, pp. 887–894.

[21] Richtmyer, R. D. and Morton, K. W., *Difference Methods for Initial-Value Problems*, Wiley, New York, 1967, pp. 302–303.

[22] MacCormack, R. W., "The Effect of Viscosity in Hypervelocity Impact Cratering," AIAA Paper 69-354, Cincinnati, Ohio, 1969.

[23] Miller, W. D., Schindel, L., and Ruetenik, J. R., "Computer Program for the Calculation of the Interaction of a Blast Wave with a Non-Uniform Shock Layer," MIT Rept. ASRL-TR-121-2, Sept. 1964, MIT, Cambridge, Mass.

[24] Hayes, W., "Approximations for Shock-Shock Interactions at Near Normal Incidence," Working Paper 72-18, Jan. 1973, Aeronautical Research Associates of Princeton, Princeton, N.J.